Large-scale instabilities in a nonrotating turbulent convection

Tov Elperin,[a)] Ilia Golubev,[b)] Nathan Kleeorin,[c)] and Igor Rogachevskii[d)]
Pearlstone Center for Aeronautical Engineering Studies, Department of Mechanical Engineering,
Ben-Gurion University of the Negev, POB 653, Beer-Sheva 84105, Israel

A theoretical approach proposed by Elperin *et al.* [Phys. Rev. E **66**, 066305 (2002)] is developed further to investigate formation of large-scale coherent structures in a nonrotating turbulent convection via excitation of a large-scale instability. In particular, the convective-wind instability that causes formation of large-scale coherent motions in the form of cells, can be excited in a shear-free regime. It was shown that the redistribution of the turbulent heat flux due to nonuniform large-scale motions plays a crucial role in the formation of the coherent large-scale structures in the turbulent convection. The modification of the turbulent heat flux results in strong reduction of the critical Rayleigh number (based on the eddy viscosity and turbulent temperature diffusivity) required for the excitation of the convective-wind instability. The large-scale convective-shear instability that results in the formation of the large-scale coherent motions in the form of rolls stretched along imposed large-scale velocity, can be excited in the sheared turbulent convection. This instability causes the generation of convective-shear waves propagating perpendicular to the convective rolls. The mean-field equations that describe the convective-wind and convective-shear instabilities, are solved numerically. We determine the key parameters that affect formation of the large-scale coherent structures in the turbulent convection. In particular, the degree of thermal anisotropy and the lateral background heat flux strongly modify the growth rates of the large-scale convective-shear instability, the frequencies of the generated convective-shear waves, and change the thresholds required for the excitation of the large-scale instabilities. This study elucidates the origin of the large-scale circulations and rolls observed in the atmospheric convective boundary layers. © *2006 American Institute of Physics.* [DOI: 10.1063/1.2401223]

I. INTRODUCTION

Large-scale coherent structures in a nonrotating turbulent convection at very large Rayleigh numbers are observed in the atmospheric convective boundary layers,[1–12] in numerous laboratory experiments in the Rayleigh-Bénard apparatus,[13–23] and in direct numerical simulations.[24,25] Spatial scales of the large-scale coherent structures in a turbulent convection are much larger than turbulent scales and their lifetimes are larger than the largest time scales of turbulence. In the atmospheric shear-free convection, the structures (cloud cells) represent large, three-dimensional, long-lived Bénard-type cells composed of narrow uprising plumes and wide downdrafts. They usually embrace the entire convective boundary layer (of the order of $1-3$ km in height) and include pronounced convergence flow patterns close to the surface. In the sheared convective flows, the structures represent large-scale rolls (cloud streets) stretched along the mean wind.[1,2,12]

Coherent structures in convective turbulent flows were comprehensively studied theoretically, experimentally, and in numerical simulations.[1–28] However, some aspects related to the origin of large-scale coherent structures in nonrotating turbulent convection are not completely understood. Hartlep

et al. (2003) noted that there are two points of view on the origin of large-scale circulation in turbulent convection.[24] "According to one point of view, the rolls which develop at low Rayleigh numbers near the onset of convection continually increase their size as Rayleigh number is increased and continue to exist in an average sense at even the highest Rayleigh numbers reached in the experiments.[29] Another hypothesis holds that the large-scale circulation is a genuine high Rayleigh number effect."[13]

Recently, a new mean-field theory of nonrotating turbulent convection has been developed.[30,31] This theory predicts the convective-wind instability in the shear-free turbulent convection that results in the formation of large-scale motions in the form of cells. In the sheared convection, the large-scale instability causes generation of convective-shear waves. The dominant coherent structures in this case are rolls. It was demonstrated[30,31] that a redistribution of the turbulent heat flux due to nonuniform large-scale motions plays a crucial role in the formation of the large-scale coherent structures in turbulent convection.

In this study, a theoretical approach[30,31] is developed further to investigate the formation of the coherent structures in the nonrotating turbulent convection. In particular, we investigated how the modification of the turbulent heat flux due to nonuniform large-scale motions affects the critical Rayleigh number (based on the eddy viscosity and turbulent thermal conductivity) required for the excitation of the convective-wind instability. We performed a numerical study of the

---

a)Electronic address: elperin@bgu.ac.il
b)Electronic address: golubev@bgu.ac.il
c)Electronic address: nat@bgu.ac.il
d)Electronic address: gary@bgu.ac.il

convective-wind and convective-shear instabilities in order to determine key parameters that affect formation of the large-scale coherent structures in the turbulent convection.

The paper is organized as follows. In Sec. II we discuss the physics of the formation of the large-scale coherent structures and formulate the mean-field equations that describe the formation of the coherent structures. In Sec. III we determine the critical Rayleigh number required for the excitation of the convective-wind instability in a shear-free turbulent convection. In Sec. IV we study numerically the convective-shear instability in a sheared convection. Finally, conclusions are drawn in Sec. V.

II. TURBULENT HEAT FLUX AND MEAN-FIELD EQUATIONS

In this section we discuss a redistribution of the turbulent heat flux due to the nonuniform large-scale motions as a key mechanism for the formation of the large-scale coherent structures in turbulent convection. Here we also formulate the mean-field equations that describe the formation of the coherent structures. Traditional theoretical models of the boundary-layer turbulence, such as the Kolmogorov-type local closures, imply the following assumptions. Fluid flows are decomposed into organized mean motions and turbulent flow. Turbulent fluxes are assumed to be proportional to the local mean gradients, whereas the proportionality coefficients (eddy viscosity, turbulent temperature diffusivity) are uniquely determined by local turbulent parameters. For example,[32] the turbulent heat flux reads $\mathbf{F} \equiv \langle s\mathbf{u} \rangle = -\kappa_T \boldsymbol{\nabla} S$, where κ_T is the turbulent temperature diffusivity, S is the mean entropy, and $\mathbf{u}$ and s are fluctuations of the velocity and entropy, respectively. This turbulent heat flux $\mathbf{F}$ does not include the contribution from anisotropic velocity fluctuations.

Actually, the mean-velocity gradients can directly affect the turbulent heat flux. The reason is that additional essentially anisotropic velocity fluctuations are generated by tangling the mean-velocity gradients with the Kolmogorov-type turbulence due to the influence of the inertial forces during the life time of large turbulent eddies. The Kolmogorov-type turbulence supplies energy to the anisotropic velocity fluctuations that cause formation of coherent structures due to the excitation of a large-scale instability.[30,31] Anisotropic velocity fluctuations are characterized by a steeper spectrum than the Kolmogorov-type turbulence.[30,33–36]

The theoretical model[30] of the anisotropic velocity fluctuations and their effect on the turbulent heat flux includes the following steps in the derivations: applying the spectral closure, solving the equations for the second moments in the **k**-space, and returning to the physical space to obtain formulas for the Reynolds stresses and the turbulent heat flux. The derivation are based on the Navier-Stokes equation and the entropy evolution equation formulated in the Boussinesq approximation. This derivation[30] yields the following expression for the turbulent heat flux $\mathbf{F} \equiv \langle s\mathbf{u} \rangle$:

$$\mathbf{F} = \mathbf{F}^* - \tau_0 \left[\alpha \mathbf{F}_z^* \operatorname{div} \mathbf{U}_\perp - \frac{1}{5}\left(\alpha + \frac{3}{2}\right)(\mathbf{W} \times \mathbf{F}_z^*) \right.$$
$$\left. - \frac{1}{2}(\mathbf{W}_z \times \mathbf{F}^*) \right], \tag{1}$$

where τ_0 is the correlation time of turbulent velocity corresponding to the maximum scale of turbulent motions, $\mathbf{W} = \boldsymbol{\nabla} \times \mathbf{U}$ is the mean vorticity, $\mathbf{U} = \mathbf{U}_\perp + \mathbf{U}_z$ is the mean velocity with the horizontal $\mathbf{U}_\perp$ and vertical $\mathbf{U}_z$ components, α is the degree of thermal anisotropy, and

$$F_i^* = -\kappa_{ij}\nabla_j S - \tau_0 F_z^* \nabla_z U_i^{(0)}(z) \tag{2}$$

is the background turbulent heat flux that is the sum of the contribution due to the Kolmogorov-type turbulence [described by the first term in Eq. (2)] and a contribution of the anisotropic turbulence caused by the shear of the imposed large-scale mean velocity $\mathbf{U}^{(0)}(z)$ [the so-called counter-wind heat flux described by the second term in Eq. (2)],

$$\kappa_{ij} = \kappa_T[\delta_{ij} + be_i e_j] \tag{3}$$

is a generalized anisotropic turbulent temperature diffusivity tensor. For turbulent convection, $b = (3/2)(2 + \tilde{\gamma})$, $\tilde{\gamma}$ is the ratio of specific heats (e.g., $\tilde{\gamma} = 7/5$ for the air flow) and $\mathbf{e}$ is the vertical unit vector. The equation for the tensor κ_{ij} was derived in Appendix A in Ref. 30 using the budget equations for the turbulent kinetic energy, fluctuations of the entropy and the turbulent heat flux. The anisotropic part of the tensor κ_{ij} [described by the second term in the square brackets of Eq. (3)], is caused by a modification of the turbulent heat flux by the buoyancy effects. Note that for a laminar convection b is set to zero and the coefficient of the turbulent temperature diffusivity κ_T should be replaced by the coefficient of the molecular temperature diffusivity. The parameter α in Eq. (1) is given by

$$\alpha = \frac{1 + 4\xi}{1 + \xi/3}, \quad \xi = \left(\frac{l_\perp}{l_z}\right)^{2/3} - 1, \tag{4}$$

where $l_\perp$ and l_z are the horizontal and vertical scales, respectively, in which the background turbulent heat flux $F_z^*(\mathbf{r}) = \langle s(\mathbf{x})u_z(\mathbf{x}+\mathbf{r})\rangle$ tends to zero. The parameter ξ describes the degree of thermal anisotropy. In particular, in isotropic case when $l_\perp = l_z$ the parameter $\xi = 0$ and $\alpha = 1$. For $l_\perp \ll l_z$, the parameter $\xi = -1$ and $\alpha = -9/2$. The maximum value ξ_{max} of the parameter ξ is given by $\xi_{max} = 2/3$ for $\alpha = 3$. The upper limit for the parameter ξ arises because the function $F_z^*(\mathbf{r})$ has a global maximum at $\mathbf{r} = 0$. Depending on the parameter α, the small-scale thermal structures in the background turbulent convection have the form of columns or pancakes (sometimes they are called small-scale thermal plumes). For $\alpha < 1$, the small-scale thermal structures have the form of columns ($l_\perp < l_z$), and for $\alpha > 1$ there exist pancake thermal structures ($l_\perp > l_z$) in the background turbulent convection (i.e., a turbulent convection with zero gradients of the mean velocity).

The terms in the square brackets in the right-hand side of Eq. (1) result from the anisotropic turbulence and depend on the ″mean″ (including coherent) velocity gradients. These terms lead to the excitation of large-scale instability and for-

mation of coherent structures. In Eq. (1), the terms with zero divergence are omitted, because only div **F** contributes to the mean-field dynamics. Neglecting the anisotropic turbulence term in Eq. (1) recovers the traditional equation for the turbulent heat flux.

The physical meaning of Eq. (1) is the following. The first term $\propto -\tau_0 \alpha \mathbf{F}_z^* \, \mathrm{div}\, \widetilde{\mathbf{U}}_\perp$ in square brackets in Eq. (1) describes the redistribution of the vertical background turbulent heat flux $\mathbf{F}_z^*$ by the perturbations of the convergent (or divergent) horizontal mean flows $\widetilde{\mathbf{U}}_\perp$. This redistribution of the vertical turbulent heat flux occurs during the lifetime of turbulent eddies. The second term $\propto \tau_0(\alpha+3/2)(\widetilde{\mathbf{W}} \times \mathbf{F}_z^*)$ in square brackets in Eq. (1) determines the formation of the horizontal turbulent heat flux due to "rotation" of the vertical background turbulent heat flux $\mathbf{F}_z^*$ by the perturbations of the horizontal mean vorticity $\widetilde{\mathbf{W}}_\perp$. The last term $\propto \tau_0(\widetilde{\mathbf{W}}_z \times \mathbf{F}^*)$ in square brackets in Eq. (1) describes the formation of the horizontal heat flux through the "rotation" of the horizontal background heat flux $\mathbf{F}_\perp^*$ (the "counter-wind" heat flux in Eq. (2)) by the perturbations of the vertical component of the mean vorticity $\widetilde{\mathbf{W}}_z$. These three effects are determined by the local inertial forces in inhomogeneous mean flows. A more detailed discussion of Eq. (1) is given in Secs. III and IV.

The counter-wind turbulent heat flux (in the direction opposite to the mean wind) is well known in the atmospheric physics and arises due to the following reason. In the sheared turbulent convection an ascending fluid element has larger temperature then that of surrounding fluid and smaller horizontal fluid velocity, while a descending fluid element has smaller temperature and larger horizontal fluid velocity. This causes the background turbulent heat flux $\mathbf{F}_\perp^* = -\tau_0 F_z^* \nabla_z \mathbf{U}_\perp^{(0)}$ in the direction opposite to the background horizontal mean sheared fluid velocity $\mathbf{U}_\perp^{(0)}(z)$.

We use the mean-field approach whereby the small-scale turbulent convection is parametrized. This is the reason we do not explicitly use thermal plumes in the consideration. The main reason for the appearance of the large-scale coherent structures is related to the modification of the heat flux by the nonuniform mean flows. The thermal plumes contribute to the modification of the turbulent heat flux. To some extent, the redistribution of the turbulent heat flux can be interpreted as a redistribution of the thermal plumes.

In order to study the formation of the large-scale coherent structures in a small-scale nonrotating turbulent convection we used the mean-field Navier-Stokes equation and the mean entropy evolution equation [with the turbulent heat flux (1)] formulated in the Boussinesq approximation. These mean-field equations yield the following linearized equations for the small perturbations from the equilibrium, $\widetilde{U} = U_z - U_z^{(0)}$, $\widetilde{W} = W_z - W_z^{(0)}$, and $\widetilde{S} = S - S^{(0)}$:

$$\left(\frac{\partial}{\partial t} + U_y^{(0)} \nabla_y - \nu_T \Delta \right) \Delta \widetilde{U} = g \Delta_\perp \widetilde{S}, \tag{5}$$

$$\left(\frac{\partial}{\partial t} + U_y^{(0)} \nabla_y - \nu_T \Delta \right) \widetilde{W} = -\sigma \nabla_x \widetilde{U}, \tag{6}$$

$$\left(\frac{\partial}{\partial t} + U_y^{(0)} \nabla_y \right) \widetilde{S} = -(\boldsymbol{\nabla} \cdot \widetilde{\mathbf{F}}) - (\nabla_z S^{(0)}) \widetilde{U}, \tag{7}$$

where ν_T is the eddy viscosity, $\Delta_\perp = \Delta - \nabla_z^2$, and

$$\boldsymbol{\nabla} \cdot \widetilde{\mathbf{F}} = -\frac{4\tau_0}{45} \{ (\mathbf{F}^* \cdot \mathbf{e})[10\alpha\Delta_\perp - (8\alpha-3)\Delta]\widetilde{U}$$
$$+ 6[(\mathbf{F}^* \times \mathbf{e}) \cdot \boldsymbol{\nabla}]\widetilde{W} \} - \kappa_T(\Delta + b\nabla_z^2)\widetilde{S}, \tag{8}$$

κ_T is the turbulent temperature diffusivity. In order to derive Eq. (5), the pressure term was excluded by calculating the curl of the momentum equation. Equations (5)–(7) allow us to study the linear stage of the large-scale instabilities. The variables $\widetilde{U}$, $\widetilde{W}$, and $\widetilde{S}$ describe the large-scale coherent structures. In Sec. III we study a shear-free convection with $\mathbf{U}^{(0)} = 0$, and in Sec. IV we investigate turbulent convection with the background (equilibrium) large-scale velocity shear $\mathbf{U}^{(0)}(z) = \sigma z \mathbf{e}_y$ and the background mean vorticity $\mathbf{W}^{(0)} = \boldsymbol{\nabla} \times \mathbf{U}^{(0)} = -\sigma \mathbf{e}_x$.

III. SHEAR-FREE CONVECTION

Let us consider a shear-free convection ($\mathbf{U}^{(0)} = 0$). In the shear-free regime, the large-scale instability is related to the first term $\propto -\tau_0 \alpha \mathbf{F}_z^* \, \mathrm{div}\, \widetilde{\mathbf{U}}_\perp$ in square brackets in Eq. (1) for the turbulent heat flux.[30,31] When $\partial \widetilde{U}_z/\partial z > 0$, perturbations of the vertical velocity $\widetilde{U}_z$ cause negative divergence of the horizontal velocity, $\mathrm{div}\, \widetilde{\mathbf{U}}_\perp < 0$ (provided that $\mathrm{div}\, \widetilde{\mathbf{U}} = 0$). This strengthens the local vertical turbulent heat flux and causes increase of perturbations of the local mean entropy and buoyancy. The latter enhances perturbations of the local mean vertical velocity $\widetilde{U}_z$, and by this means, the convective-wind instability is excited. Similar reasoning is valid when $\partial \widetilde{U}_z/\partial z < 0$, whereas $\mathrm{div}\, \widetilde{\mathbf{U}}_\perp > 0$. Negative perturbations of the vertical flux of entropy then lead to a decrease of perturbations of the mean entropy and buoyancy, which enhances the downward flow and once again excites the convective-wind instability. Therefore, nonzero $\mathrm{div}\, \widetilde{\mathbf{U}}_\perp$ causes redistribution of the vertical turbulent heat flux and formation of regions with large values of this flux. These regions (where $\mathrm{div}\, \widetilde{\mathbf{U}}_\perp < 0$) alternate with the low heat flux regions (where $\mathrm{div}\, \widetilde{\mathbf{U}}_\perp > 0$). This process results in formation of the large-scale coherent structures.

The role of the second term $\propto \tau_0(\alpha+3/2)(\widetilde{\mathbf{W}} \times \mathbf{F}_z^*)$ in square brackets in Eq. (1) is to decrease the growth rate of the large-scale instability for $\alpha > -3/2$. Indeed, the interaction of perturbations of the mean vorticity with the vertical background turbulent heat flux $\mathbf{F}_z^*$ produces the horizontal turbulent heat flux. The latter decreases (increases) the mean entropy in the regions with upward (downward) local flows, thus diminishing the buoyancy forces and reducing the mean vertical velocity $\widetilde{U}_z$ and the mean vorticity $\widetilde{\mathbf{W}}$. This mechanism dampens the convective-wind instability for $\alpha > -3/2$. The above two competitive effects determine the growth rate of the convective-wind instability. A solution of Eqs. (5) and (7) in the shear-free convection regime yields the following expression for the growth rate γ of long-wave perturbations:

$$\gamma \propto g F_z^* \tau_0^2 K^2 \sqrt{\beta} |\sin \theta| \left[\alpha - \frac{3}{8} - \frac{5\alpha}{4} \sin^2 \theta \right]^{1/2}, \qquad (9)$$

where the parameter $\beta = (l_0 K)^{-2} \gg 1$, l_0 is the maximum scale of turbulent motions, θ is the angle between the vertical unit vector **e** and the wave vector **K** of small perturbations, and **g** is acceleration of gravity. The analysis of the convective-wind instability was performed in Refs. 30 and 31 only for a small square of Brunt-Väisälä frequency. In particular, Eq. (9) was derived in Refs. 30 and 31 for the case $|N^2| \ll g F_z^* \tau_0 K^2$, where $N^2 = -(\mathbf{g} \cdot \boldsymbol{\nabla}) S^{(0)} < 0$ is the square of Brunt-Väisälä frequency.

In the present study we consider arbitrary values of the Brunt-Väisälä frequency, and we investigate the effect of the modification of the turbulent heat flux (due to nonuniform large-scale motions) on the critical effective Rayleigh number required for the excitation of the convective-wind instability. We also study here the effect of the anisotropy of turbulent thermal diffusivity (caused by the buoyancy) on the critical effective Rayleigh number. To this end, we rewrite Eqs. (5) and (7) in a nondimensional form:

$$\left(\frac{\partial}{\partial t} - \Delta \right) \Delta V = \text{Ra} \, \Delta_{\perp} \widetilde{S}, \qquad (10)$$

$$\text{Pr}_T \frac{\partial \widetilde{S}}{\partial t} - (\Delta + b \nabla_z^2) \widetilde{S} = V + \mu \left(\frac{\text{Pr}_T}{\text{Ra}} \right)^{1/3}$$
$$\times [10\alpha\Delta_{\perp} - (8\alpha - 3)\Delta] V, \qquad (11)$$

where $V = \text{Pr}_T \zeta \Lambda \widetilde{U}$ is dimensionless velocity, the length is measured in the units of the total vertical size L_z of the system, the parameter $b = 3(2 + \widetilde{\gamma})/2$ describes the anisotropy of turbulent thermal diffusivity caused by the buoyancy effect [see Eqs. (3)], $\text{Ra} = 6\Lambda^3 \zeta \text{Pr}_T$ is effective Rayleigh number based on the turbulent viscosity, ν_T, and the turbulent temperature diffusivity, κ_T, $\Lambda = L_z/l_0$, $\text{Pr}_T = \nu_T/\kappa_T$ is the turbulent Prandtl number, the parameter μ is given by

$$\mu = \frac{4a_*}{15} \left(\frac{6}{\zeta^2} \right)^{1/3}, \quad \zeta = \frac{6g l_0}{u_0^2} \frac{\delta T}{T_0},$$

δT is the mean temperature difference between bottom and upper boundaries of the turbulent convection, the parameter $a_* = 2g\tau_0 F_z^*/u_0^2$, and T_0 is the reference mean temperature. The last term $\propto \mu$ in the right-hand side of Eq. (11) determines the modification of the turbulent heat flux due to the nonuniform large-scale motions, and the parameter

$$\mu \left(\frac{\text{Pr}_T}{\text{Ra}} \right)^{1/3} = \frac{4g\tau_0 F_z^*}{|N^2| L_z^2}$$

has the meaning of the normalized heat flux, where $|N^2| = g\delta T/[T_0 L_z]$ and $\text{Ra} = |N^2| L_z^4/[\nu_T \kappa_T]$.

A. Solution for two free boundaries

Let us consider the solution of Eqs. (10) and (11) for two free boundaries, using the following boundary conditions
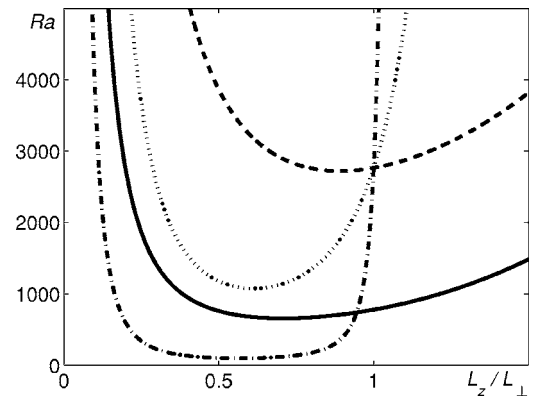

FIG. 1. Effective Rayleigh number versus the aspect ratio $L_z/L_{\perp}$ of the perturbations for two free boundaries and different values of the parameter μ: $\mu = 0$ (dashed line); for $\mu = 0.7$ (dotted line); $\mu = 5$ (dashed-dotted line). Here, $\alpha = 1$ and $b = 5.1$. The classical Rayleigh solution for the laminar convection ($b = 0$) with the two free boundaries is shown by solid curve.

$$V = \nabla_z^2 V = \widetilde{S} = 0 \quad \text{for} \quad z = 0; 1. \qquad (12)$$

We seek for a solution of Eqs. (10) and (11) in the form

$$V, \widetilde{S} \propto \sin(\pi n z) \exp(\gamma t - i \mathbf{K}_{\perp} \cdot \mathbf{r}),$$

where n is the integer number and $\mathbf{K}_{\perp}$ is the horizontal component of the wave vector. The critical effective Rayleigh number (at $\gamma = 0$) is determined by the equation

$$[K_{\perp}^2 + (b + 1)\pi^2 n^2](K_{\perp}^2 + \pi^2 n^2)^2$$
$$= K_{\perp}^2 \{ \text{Ra}_c - \mu (\text{Pr}_T \text{Ra}_c^2)^{1/3}$$
$$\times [(2\alpha + 3)K_{\perp}^2 - (8\alpha - 3)\pi^2 n^2] \},$$

where the critical effective Rayleigh number Ra_c is based on the turbulent viscosity and the turbulent temperature diffusivity.

In the case of $\mu = 0$ (i.e., there is no modification of the turbulent heat flux due to the nonuniform large-scale motions), the critical effective Rayleigh number is given by

$$\text{Ra}_c = \frac{(K_{\perp}^2 + \pi^2 n^2)^2 [K_{\perp}^2 + (b + 1)\pi^2 n^2]}{K_{\perp}^2}. \qquad (13)$$

The minimum value of the critical effective Rayleigh number for the first mode ($n = 1$) for $b = 0$ is $\text{Ra}_c \approx 657.5$. This is the classical Rayleigh solution for the laminar convection with two free boundaries. The critical effective Rayleigh number increases with the increase of the anisotropy of turbulent temperature diffusivity [see Eqs. (3)] described by the parameter b. Indeed, for $b = 3.9$, the critical effective Rayleigh number is $\text{Ra}_c \approx 2247$, and for $b = 5.1$ it is $\text{Ra}_c \approx 2722$.

The modification of the turbulent heat flux due to non-uniform large-scale motions strongly decreases the critical effective Rayleigh number. Indeed, Fig. 1 shows the effective Rayleigh number versus the aspect ratio $L_z/L_{\perp} \equiv K_{\perp}/K_z = \tan \theta$ of the perturbations for different values of parameter μ. The increase of the parameter μ causes strong reduction of the critical Rayleigh number (see Table I).

TABLE I. Critical effective Rayleigh numbers for different types of the boundaries. Here for the turbulent flow $\alpha = 1$ and $b = 5.1$. The case of laminar convection is presented in Table I only for comparison with the results obtained for the turbulent convection.

| | Boundaries | | | | | |
| | Two free | | One free and one rigid | | Two rigid | |
Case	$L_z/L_\perp$	Ra_c	$L_z/L_\perp$	Ra_c	$L_z/L_\perp$	Ra_c
Laminar flow	0.707	657.5	0.854	1101	0.994	1708
Turbulent flow						
$\mu = 0$	0.891	2722	1.096	4023	1.280	5547
$\mu = 0.7$	0.613	1076	0.697	1328	0.754	4218
$\mu = 2.0$	0.578	344	0.645	420	0.688	1743
$\mu = 5.0$	0.568	98	0.628	120	0.662	549

B. Solution for two rigid boundaries

Now let us consider the solution of Eqs. (10) and (11) for two rigid boundaries. In view of the symmetry of this problem with respect to two bounding planes, it is convenient to translate the origin of z to be midway between the two planes. Fluid is then confined between two planes $z = \pm 1/2$, and we seek for a solution of Eqs. (10) and (11) satisfying the following boundary conditions

$$V = \nabla_z V = \tilde{S} = 0 \quad \text{for} \quad z = \pm \frac{1}{2}. \tag{14}$$

We seek for the solution of Eqs. (10) and (11) in the form V, $\tilde{S} \propto \exp(\gamma t + qz - i\mathbf{K}_\perp \cdot \mathbf{r})$, where the critical effective Rayleigh number is determined by the equation

$$
\begin{aligned}
&[K_\perp^2 - (1+b)q^2](K_\perp^2 - q^2)^2 \\
&= K_\perp^2 \{Ra_c - \mu(Pr_T Ra_c^2)^{1/3} \\
&\quad \times [(2\alpha + 3)K_\perp^2 + (8\alpha - 3)q^2]\}.
\end{aligned}
\tag{15}
$$

The problem is symmetric with respect to the two boundaries so the eigenfunctions fall into two distinct classes: the even mode with vertical velocity symmetry with respect to the midplane and the odd mode with vertical velocity asymmetry. Following the procedure described in Refs. 37–39, we adopted the even solution that has minimum critical effective Rayleigh number. Our numerical analysis showed that the anisotropy of turbulent temperature diffusivity described by the parameter b increases the critical effective Rayleigh number. In particular, for $b = 0$ the critical effective Rayleigh number is $Ra_c \approx 1707.8$. This is classical Rayleigh solution for the laminar convection with the two rigid boundaries. For $\mu = 0$ and $b = 3.9$, the critical effective Rayleigh number is $Ra_c \approx 4683$, and for $b = 5.1$ it is $Ra_c \approx 5547$.

The effective Rayleigh number versus the aspect ratio $L_z/L_\perp$ of the perturbations for two rigid boundaries is plotted in Fig. 2. Increasing of the parameter μ decreases both the critical effective Rayleigh number and the aspect ratio $L_z/L_\perp$ of perturbations (see Table I). If $\mu \geq 5$, the behavior of the effective Rayleigh number drastically changes; i.e., there are two local minima for the effective Rayleigh number.

C. Solution for one rigid and one free boundaries

Solution for one rigid and one free boundary can be obtained from the results for two rigid boundaries using the odd mode. We use the domain from $z = 0$ (the free boundary) to $z = 1/2$ (the rigid boundary). The anisotropy of turbulent temperature diffusivity described by the parameter b increases the critical effective Rayleigh number. Indeed, for $b = 0$, the critical effective Rayleigh number is $Ra_c \approx 1101$ (the classical Rayleigh solution for the laminar convection). For $\mu = 0$ and $b = 3.9$, the critical effective Rayleigh number is $Ra_c \approx 3359$, and for $b = 5.1$ it is $Ra_c \approx 4023$. The effective Rayleigh number versus the aspect ratio $L_z/L_\perp$ of the perturbations for the one rigid and one free boundary is plotted in Fig. 3. Increasing the parameter μ decreases the critical effective Rayleigh number and reduces the aspect ratio $L_z/L_\perp$ of the perturbations (see Table I).

Therefore, for these three types of boundaries the modification of the turbulent heat flux due to the nonuniform large-scale motions strongly reduces the critical effective Rayleigh number (based on the eddy viscosity and turbulent temperature diffusivity) required for the excitation of the convective-wind instability. We summarized the final results for the above three types of the boundary conditions in Table
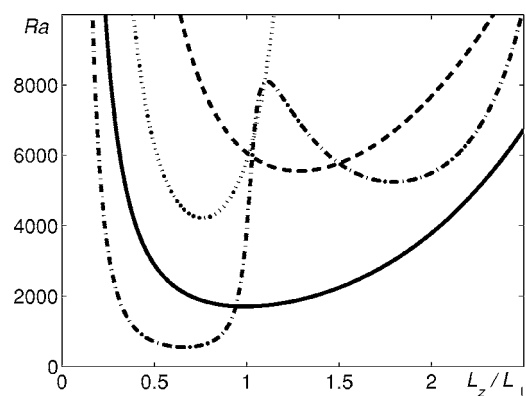

FIG. 2. Effective Rayleigh number versus the aspect ratio $L_z/L_\perp$ of the perturbations for two rigid boundaries and different values of the parameter μ: $\mu = 0$ (dashed line); $\mu = 0.7$ (dotted line); $\mu = 5$ (dashed-dotted line). Here, $\alpha = 1$ and $b = 5.1$. The classical Rayleigh solution for the laminar convection ($b = 0$) with the two rigid boundaries is shown by the solid curve.
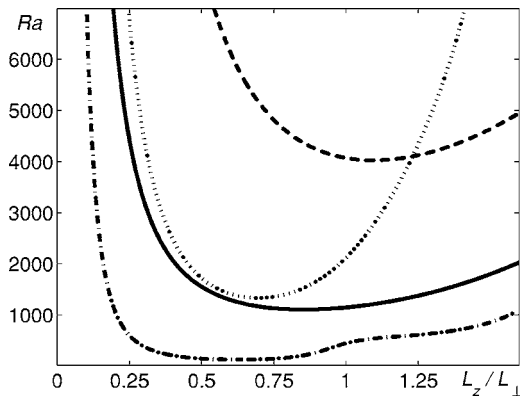
FIG. 3. Effective Rayleigh number versus the aspect ratio $L_z/L_\perp$ of the perturbations for one rigid and one free boundary and different values of the parameter μ: $\mu=0$ (dashed line); $\mu=0.7$ (dotted line); $\mu=5$ (dashed-dotted line). Here, $\alpha=1$ and $b=5.1$. The classical Rayleigh solution for the laminar convection ($b=0$) with one rigid and one free boundary is shown by solid curve.

I. The case of laminar convection is presented in Table I only for comparison with the results obtained for the turbulent convection.

IV. SHEARED TURBULENT CONVECTION

In this section we consider turbulent convection with a large-scale linear velocity shear $\mathbf{U}^{(0)}(z)=\sigma z\mathbf{e}_y$. In a sheared turbulent convection the mechanism of the convective-shear instability[30,31] is related to the last term $\propto\tau_0(\widetilde{\mathbf{W}}_z\times\mathbf{F}^*)$ in square brackets in Eq. (1). The generation of the potential temperature perturbations by vorticity perturbations plays the key role in this mechanism. Indeed, in two adjacent vortices with the opposite directions of the vertical vorticity $\widetilde{\mathbf{W}}_z$, the turbulent fluxes of potential temperature are directed towards the boundary between the vortices. This increases perturbations of the mean potential temperature and the buoyancy, and generates the upward flow between the vortices. These vertical flows excite vorticity perturbations, and the convective-shear instability mechanism is sustained.

Let us consider an evolution of perturbations with zero y-derivatives of the fields $\widetilde{U}$, $\widetilde{W}$, and $\widetilde{S}$. We seek for a solution of Eqs. (5)–(7) in the form $\propto\exp(\gamma t-i\mathbf{K}\cdot\mathbf{r})$. The growth rate of the convective-shear instability of long-wave perturbations is given by[30,31]

$$\gamma \propto gF_z^*\tau_0^2K^2(\beta\lambda\sin^2\theta)^{2/3}, \qquad (16)$$

where $\lambda=\sigma\tau_0$ is the shear parameter, the parameter $\beta\equiv(l_0K)^{-2}\gg1$ and $K=\sqrt{K_x^2+K_z^2}$. The convective-shear instability causes formation of large-scale coherent fluid motions in the form of rolls (see Fig. 4) aligned along the imposed mean velocity $\mathbf{U}^{(0)}$. The instability can also result in generation of the convective-shear waves with the frequency

$$\Omega \propto \sqrt{3}gF_z^*\tau_0^2K^2(\beta\lambda\sin^2\theta)^{2/3}, \qquad (17)$$

which implies the wave-number dependence $\Omega\propto K^{2/3}$. The convective-shear waves propagate perpendicular to convective rolls (see Fig. 4). The analysis of the convective-shear instability was performed in Refs. 30 and 31 only for a small

square of Brunt-Väisälä frequency and zero y-derivatives of the fields $\widetilde{U}$, $\widetilde{W}$, and $\widetilde{S}$. This corresponds to the convective-shear instability for a very small component of the wave number along the imposed mean shear (i.e., uniform perturbations along the large-scale shear velocity). In this case the growth rate of the convective-shear instability is maximum.

In the present study we consider arbitrary values of the Brunt-Väisälä frequency and perform the numerical analysis of the convective-shear instability for nonzero y-derivatives of the fields $\widetilde{U}$, $\widetilde{W}$, and $\widetilde{S}$. We consider the eigenvalue problem with boundary conditions. We seek for a solution of Eqs. (5)–(7) in the form $\propto\Psi(z)\exp(\gamma t-i\mathbf{K}_\perp\cdot\mathbf{r})$, where the eigenfunction $\Psi(z)$ and the growth rate γ of the convective-shear instability are determined by Eqs. (5)–(7). The system of the ordinary differential equations for the eigenvalue problem is solved numerically with the following boundary conditions: $\widetilde{U}=\widetilde{U}''=\widetilde{U}^{IV}=\widetilde{W}=\widetilde{S}=0$ at $z=0$, and $\widetilde{U}'=\widetilde{W}'=\widetilde{S}'=0$ at $z=1$, where $f'=df/dz$. We also take into account that for a turbulent convection, the turbulent Prandtl number can be estimated as $Pr_T^{-1}\approx4/(1+Pr)\approx2.34$ with $Pr=0.71$ (for air flow). The latter estimate follows from the balance equations for the turbulent heat flux, the entropy fluctuations and the turbulent kinetic energy.[30]

Let us consider the thermally isotropic ($\alpha=1$) turbulent convection. Figure 5 shows the range of parameters
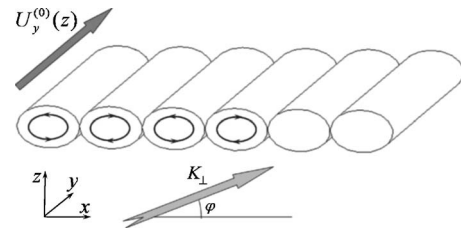

FIG. 4. Large-scale coherent rolls formed due to the convective-shear instability and aligned along the sheared mean velocity $\mathbf{U}^{(0)}(z)$. The instability results in generation of the convective-shear waves which propagate perpendicular to the convective rolls.
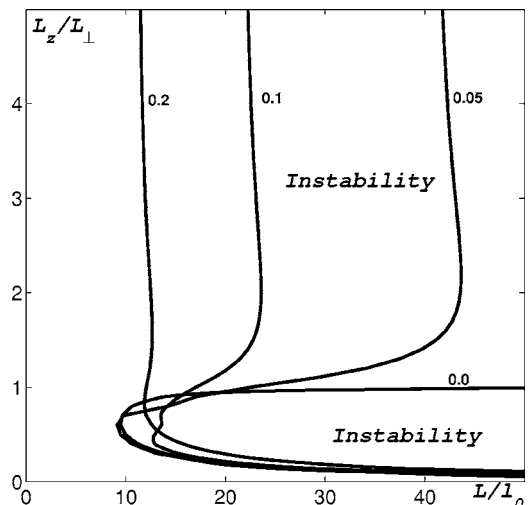

FIG. 5. Range of parameters ($L_z/L_\perp$; L/l_0) for which the convective-shear instability occurs, for different values of the shear parameter $\lambda=0$; 0.05; 0.1; 0.2. Here, $\alpha=1$.
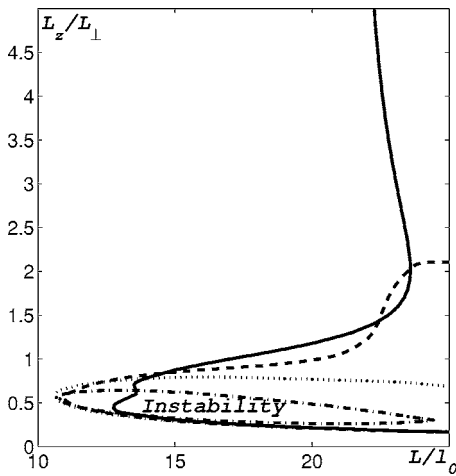
FIG. 6. Range of parameters $(L_z/L_\perp; L/l_0)$ for which the convective-shear instability occurs, for different values of the angle φ between the horizontal wave vector and the x axis: $\varphi=0°$ (solid line); $\varphi=18°$ (dashed line); $\varphi=30°$ (dotted line); $\varphi=90°$ (dashed-dotted line). Here, $\alpha=1$ and $\lambda=0.1$.

FIG. 7. Growth rates of the convective-shear instability and the frequencies of the generated convective-shear waves versus: $L_z/L_\perp$ and L/l_0. Corresponding dependencies on the parameters L/l_0 are given for different $L_z/L_\perp$ and vice versa. Here, $\alpha=1$ and $\lambda=0.1$.

$(L_z/L_\perp; L/l_0)$, for which the convective-shear instability occurs for different values of the shear parameter λ. Here, $L\equiv 1/\sqrt{L_z^{-2}+L_\perp^{-2}}$, and we assumed that $a_*=1$. The case $\lambda=0$ in Fig. 5 corresponds to the convective-wind instability (the shear-free turbulent convection). Inspection of Fig. 5 shows that the increase of shear is favorable for the excitation of the convective-shear instability. In Fig. 6 we plotted the range of parameters $(L_z/L_\perp; L/l_0)$ for the convective-shear instability for different values of the angle φ between the horizontal wave vector $\mathbf{K}_\perp$ and the x axis. Increasing the angle φ prevents from the excitation of the convective-shear instability (i.e., reduces the range of param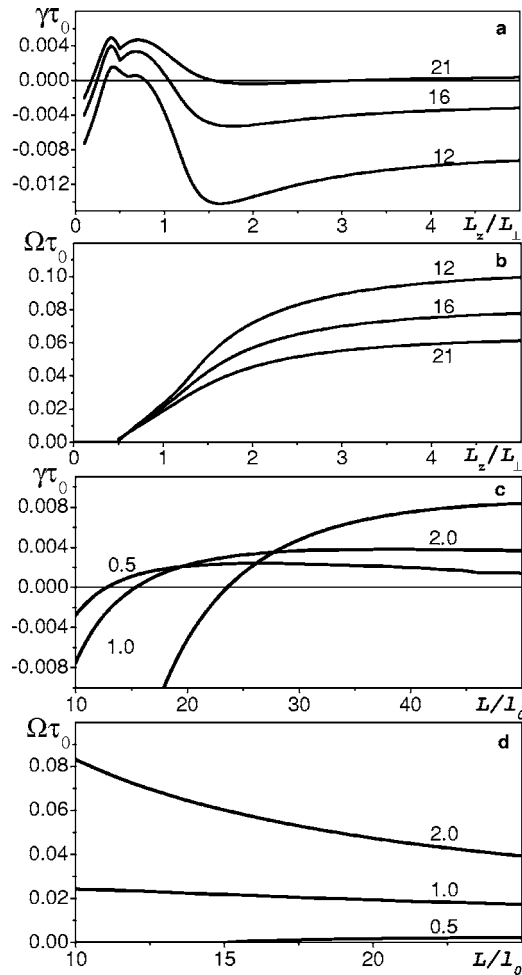eters for which the instability occurs). In Fig. 7 we plotted the growth rates of the convective-shear instability and the frequencies of the generated convective-shear waves versus $L_z/L_\perp$ and L/l_0. The curves in Fig. 7 have a point L_* whereby the first derivative $d\gamma/dK$ has a singularity, which is indicative of bifurcation. The growth rate of the convective-shear instability for very small y-derivatives of the fields $\tilde{U}$, $\tilde{W}$, and $\tilde{S}$, is determined by cubic algebraic equation.[30] Below the bifurcation point, the cubic equation has three real roots (which corresponds to aperiodic instability without generation of waves). Above the bifurcation point, the cubic equation has one real and two complex conjugate roots. In this case the convective-shear waves are generated. The source of energy for these waves is the turbulence energy.

Now we perform the detailed numerical analysis of the convective-shear instability in order to determine the key parameters that affect this instability. First, we study the effect of the thermal anisotropy α on the convective-shear instability. Figure 8 shows the range of parameters $(L_z/L_\perp; L/l_0)$ for which the convective-shear instability occurs, for different values of the thermal anisotropy α. In Fig. 9 we plotted the growth rates of the convective-shear instability and the frequencies of the generated convective-shear waves for different values of α. The decrease of the degree of thermal anisotropy α increases the threshold in the parameter L/l_0 required for the excitation of the convective-shear insta-

bility. Figure 10 shows the growth rates of the convective-shear instability versus the angle φ between the horizontal wave vector $\mathbf{K}_\perp$ and the x axis for different values of α. Here, the values $L_z/L_\perp$ and L/l_0 correspond to the maximum growth rates of the instability. For $\alpha>0.7$ the growth rate of the convective-shear instability attains the maximum for $\varphi_m>0°$. An increase of the degree of thermal anisotropy α increases the angle φ_m. In the thermally isotropic ($\alpha=1$) turbulent convection the angle $\varphi_m=18°$, while for $\alpha=0.8$ (i.e., $\xi\approx0.92$), the angle $\varphi_m\approx10°$. Note that according to the atmospheric observations, the observed angle between the cloud streets and direction of the wind is of the order of $10°$–$14°$. The calculated angle φ_m is in compliance with these observations. Note that the convective rolls are stretched in the horizontal plane in the direction perpendicular to $\mathbf{K}_\perp$ and the shear velocity is directed along the y axis. Inspection of Figs. 9 and 10 shows that decrease of the parameter α reduces the growth rates of the convective-shear instability. In Figs. 8–10 we considered the case $\alpha\lesssim1$, which is of interest in view of the atmospheric applications.

Next, we study the effect of the lateral background heat flux {determined by the third term $\propto[(\mathbf{F}^*\times\mathbf{e})\cdot\boldsymbol{\nabla}]\tilde{W}$ in
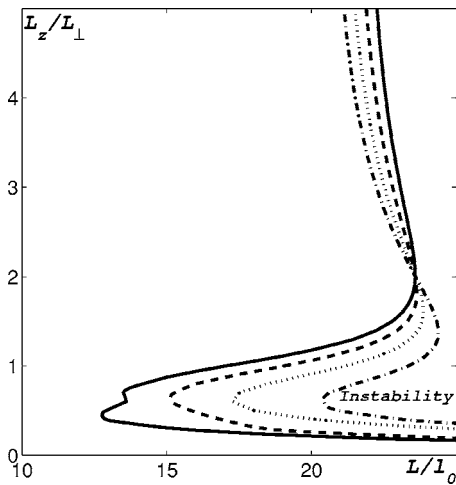
FIG. 8. Range of parameters $(L_z/L_\perp; L/l_0)$ for which the convective-shear instability occurs, for $\lambda=0.1$ for different values of the degree of thermal anisotropy α: $\alpha=1$ (solid line); $\alpha=0.9$ (dashed line); $\alpha=0.8$ (dotted line); $\alpha=0.7$ (dashed-dotted line).

FIG. 10. Growth rates of the convective-shear instability versus the angle φ between the horizontal wave vector and the x axis for different values of the degree of thermal anisotropy α: $\alpha=1$ (solid line); $\alpha=0.9$ (dashed line); $\alpha=0.8$ (dotted line); $\alpha=0.7$ (dashed-dotted line). Here, $\lambda=0.1$; the values $L_z/L_\perp$ and L/l_0 correspond to maximum growth rates of the instability.

the right-hand side of Eq. (8)}, on the convective-shear instability. We introduce the angle ψ between the horizontal component $\mathbf{F}_\perp^*$ of the background turbulent heat flux and x axes, where the total background heat flux is $\mathbf{F}^*=(F_\perp^* \cos\psi, F_\perp^* \sin\psi, F_z^*)$. The angle ψ is determined by the boundary conditions in the horizontal plane (e.g., by the temperature gradient in the horizontal plane). Figure 11 shows the range of parameters $(L_z/L_\perp; L/l_0)$ for which the convective-shear instability occurs, for different directions ψ of the lateral background heat flux $\mathbf{F}_\perp^*$. In Figs. 12 and 13 we plotted the growth rates of the convective-shear instability and the frequencies of the generated convective-shear waves for this case, where $F_\perp^*/F_z^*=0.5$. Note that the background mean vorticity due to the imposed large-scale shear is $\mathbf{W}^{(0)}=\nabla\times\mathbf{U}^{(0)}=-\sigma\mathbf{e}_x$. This is the reason there is no symmetry with respect to the Y-Z plane of the large-scale shear; i.e., the contributions to the convective-shear instability caused

by the positive and negative angles ψ of the lateral background heat flux are different. In particular, the range of the convective-shear instability in the presence the lateral background heat flux with the positive angles ψ is wider than that for the negative angles ψ (see Fig. 11). On the other hand, even for the negative angles ψ the range of the convective-shear instability is wider than that in the absence of the lateral background heat flux. Note also that in the presence of the lateral background heat flux with the positive angles ψ, the convective-shear waves are not generated. This is reason we plotted in Figs. 12(c) and 13(c) the frequencies of the generated convective-shear waves only for $\psi\leq0$.

Note that there are three groups of parameters in this study of the large-scale coherent structures formed in a turbulent convection:

(i) the external parameters: the value of shear σ and the background heat flux $\mathbf{F}^*=(F_\perp^* \cos\psi, F_\perp^* \sin\psi, F_z^*)$;

(ii) the parameters that determine the background turbulent convection: the degree of thermal anisotropy α, the correlation time $\tau_0=l_0/u_0$, and the parameter $a_*=2g\tau_0 F_z^*/u_0^2$;
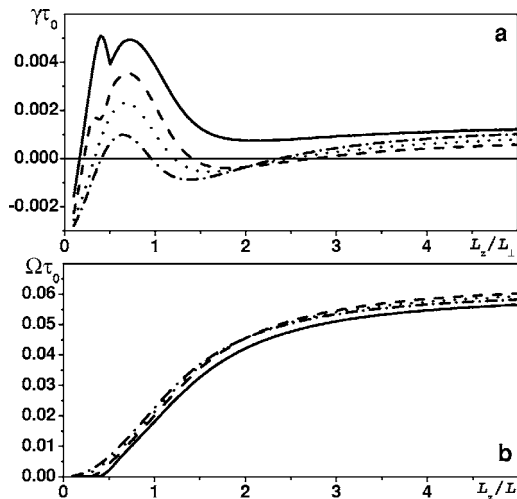

FIG. 9. Growth rates of the convective-shear instability and the frequencies of the generated convective-shear waves for different values of the degree of thermal anisotropy α: $\alpha=1$ (solid line); $\alpha=0.9$ (dashed line); $\alpha=0.8$ (dotted line); $\alpha=0.7$ (dashed-dotted line). Here $\lambda=0.1$ and $L/l_0=23$.
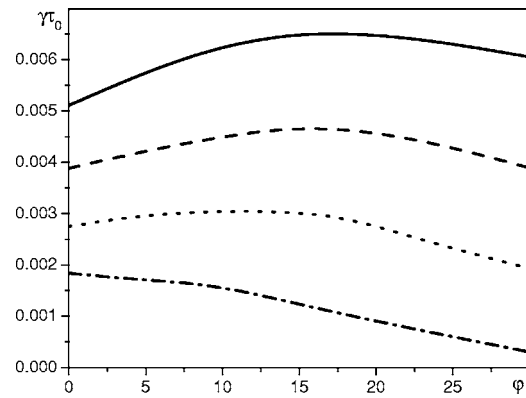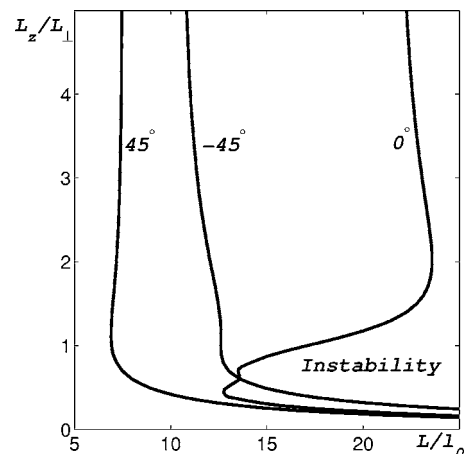

FIG. 11. Range of parameters $(L_z/L_\perp; L/l_0)$ for which the convective-shear instability occurs, for different directions ψ of the lateral background heat flux: $\psi=-45°$; $\psi=0°$; $\psi=45°$. Here, $\lambda=0.1$.
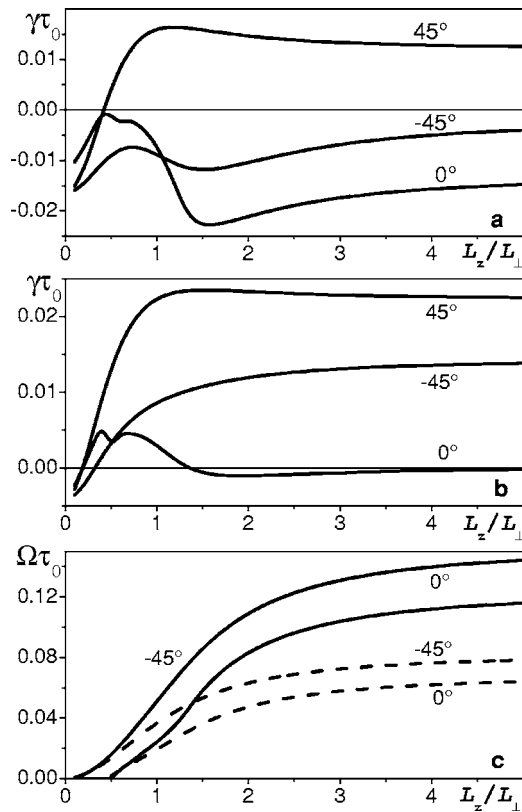
FIG. 12. Growth rates of the convective-shear instability and the frequencies of the generated convective-shear waves versus $L_z/L_\perp$ for different directions ψ of the lateral background heat flux: $\psi = -45°$; $\psi = 0°$; $\psi = 45°$. (a) The growth rates of the instability for $L/l_0 = 10$. (b) The growth rates of the instability for $L/l_0 = 20$. (c) The frequencies of the generated waves for $L/l_0 = 10$ (solid line) and $L/l_0 = 20$ (dashed line). Here, $\lambda = 0.1$.
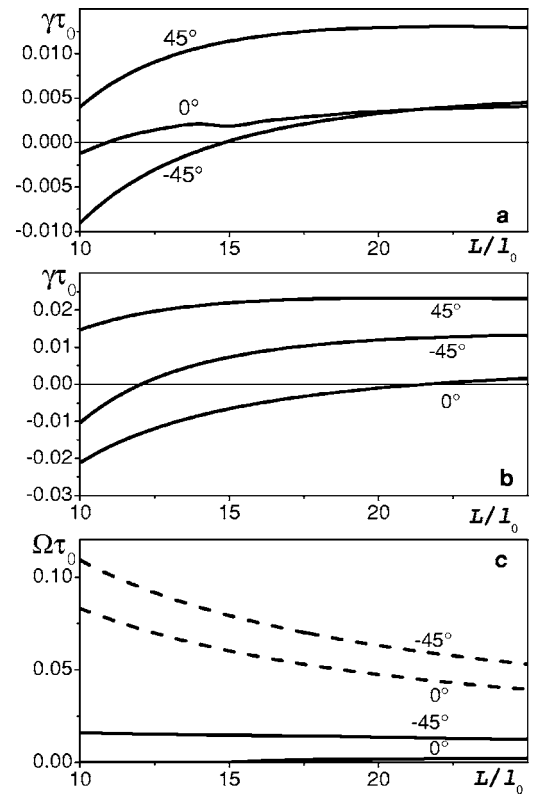

FIG. 13. Growth rates of the convective-shear instability and the frequencies of the generated convective-shear waves versus L/l_0 for different directions ψ of the lateral background heat flux: $\psi = -45°$; $\psi = 0°$; $\psi = 45°$. (a) The growth rates of the instability for $L_z/L_\perp = 0.5$. (b) The growth rates of the instability for $L_z/L_\perp = 2$. (c) The frequencies of the generated waves for $L_z/L_\perp = 0.5$ (solid line) and $L_z/L_\perp = 2$ (dashed line). Here, $\lambda = 0.1$.

(iii) the parameters related to the characteristics of the large-scale coherent structures: the aspect ratio of the structure $L_\perp/L_z$, the minimum size L of the structure, $L_x = L_\perp \cos \varphi$, the characteristic time of the formation of the large-scale coherent structures $\propto \gamma^{-1}$, and the frequency Ω of the generated convective-shear waves.

The parameters related to the characteristics of the large-scale coherent structures are determined in this study. The external parameters and the parameters that determine the background turbulent convection at the present level of analysis are treated as free parameters. The external parameters are determined by the boundary conditions. The degree of thermal anisotropy α can be determined by the budget equation for the two-point correlation function for the velocity-entropy fluctuations. This parameter has been recently measured in a laboratory experiment in turbulent convection in air-flow.[23] In the range of the Rayleigh numbers $10^7 - 10^8$ (based on the kinematic viscosity and molecular diffusivity) this parameter varies within the range from 0.5 to 2. The parameter a_* and the correlation time $\tau_0 = l_0/u_0$ can be determined from the budget equations for the turbulent kinetic energy and vertical turbulent fluxes of momentum and the entropy. The turbulent correlation time τ_0 and correlation length l_0 are measured in laboratory convection (see, e.g., Ref. 23).

V. DISCUSSION

In the present study we investigated formation of large-scale coherent structures in a nonrotating turbulent convection due to an excitation of large-scale instabilities. In the shear-free turbulent convection, the cell-like structures are formed due to the convective-wind instability. The redistribution of the turbulent heat flux due to the nonuniform large-scale motions causes strong reduction of the critical effective Rayleigh number required for the excitation of the convective-wind instability. The effective Rayleigh number is based on the eddy viscosity and turbulent thermal conductivity. We also found that the critical effective Rayleigh number increases with the increase of the anisotropy of turbulent temperature diffusivity caused by the buoyancy effects.

In the sheared turbulent convection, the roll-like structures stretched along the imposed large-scale sheared velocity are formed due to the large-scale convective-shear instability. This instability produces the convective-shear waves propagating perpendicular to the convective rolls. We studied numerically the convective-shear instability and determined the key parameters that affect the formation of the large-scale coherent structures in the turbulent convection. In particular, we found that the degree of thermal anisotropy and the lateral background heat flux strongly modify the growth rates of the large-scale convective-shear instability, the frequen-

cies of the generated convective-shear waves and change the instability thresholds.

The results described in this study are based on the linearized mean-field equations, and therefore, they cannot describe detail features of the turbulent convection observed in the numerous laboratory experiments[13–22] and in direct numerical simulations.[24,25] In particular, we made the following assumptions about the turbulent convection. We considered a homogeneous, incompressible background turbulent convection (i.e., the turbulent convection without mean-velocity gradients). The nonuniform mean velocity affects the background turbulent convection; i.e., it causes generation of the additional strongly anisotropic velocity fluctuations by tangling of the mean-velocity gradients with the background turbulent convection. We assumed that the generated anisotropic fluctuations do not affect the background turbulent convection. This implies that we considered a one-way coupling due to a weak inhomogeneity of the large-scale velocity. Thus, we studied simple physical mechanisms to describe an initial stage of the formation of large-scale coherent structures in a nonrotating turbulent convection. The simple model considered in our paper can only mimic the real flows associated with laboratory turbulent convection. Clearly, the comprehensive theoretical and numerical studies are required for quantitative description of the laboratory turbulent convection.

Although this model is very simple, it reproduces some properties of the semi-organized structures observed in the atmospheric turbulent flows.[31] The semi-organized structures are observed in the form of rolls (cloud streets) or three-dimensional convective cells (cloud cells). The observed angle between the cloud streets and the mean horizontal wind of the sheared turbulent convection is about $10°–14°$, the lengths of the cloud streets vary from 20 to 200 km, the widths from 2 to 10 km, and convective depths from 2 to 3 km. The ratio of the minimal size of the structure to the maximum scale of turbulent motions $L/l_0 = 10–100$. The characteristic lifetime of rolls varies from 1 to 72 h. Rolls may occur over water surface or land surfaces.[1,2] Our study yield the following parameters of the convective rolls: $L/l_0 = 10–100$, the characteristic time of formation of the rolls $\sim 1/\gamma$ varies from 1 to 3 h. The lifetime of the convective rolls is determined by a nonlinear evolution of the convective-shear instability. The latter is a subject of a separate ongoing study. We have shown that the maximum growth rate of the convective-shear instability is attained when the angle between the cloud streets and the mean horizontal wind of the convective layer is about $10°–17°$ in agreement with observations. We also found an excitation of the convective-shear waves propagating perpendicular to convective rolls. This finding is in agreement with observations in the atmospheric convective boundary layer, whereby the waves propagating perpendicular to cloud streets have been detected.[11] In addition, the motions in the convective rolls have a nonzero helicity in agreement with predictions made in Ref. 40.

There are two types of cloud cells in the atmospheric shear-free turbulent convection: open and closed. Open-cell circulation has downward motion and clear sky in the cell center, surrounded by cloud associated with upward motion. Closed cells have the opposite circulation.[2] Both types of cells have diameters ranging from 10 to 40 km, they occur in a convective layer with a depth of about 1 to 3 km, and the characteristic lifetime of cloud cells is about several hours. Our analysis shows that the minimum threshold value of the effective Rayleigh number required for the excitation of the large-scale instability is attained at $L_\perp/L_z = 2$ (see Figs. 1–3, dotted and dashed-dotted curves), is in agreement with numerous observations. The ratio of the minimum size of the structure to maximum scale of turbulent motions $L/l_0 = 5–15$. The characteristic time of formation of the convective cells $\sim 1/\gamma$ varies from 1 to 3 h. Therefore, the predictions of the developed theory are in agreement with observations of the semi-organized structures in the atmospheric convective boundary layer. The typical temporal and spatial scales of structures are always much larger then the turbulence scales. This justifies the separation of scales, which was assumed in the suggested in the theory. Note that the applicability of the mean-field equations for study of turbulent convection was discussed in Ref. 41.

In our study we consider nonrotating turbulent convection and apply our results to the atmospheric convective boundary layers, where the shear is usually caused by wind. The rotation of the Earth usually affects the hight of the atmospheric convective boundary layer. The rotation can also affect the longitudinal spatial structure of the cloud streets. Note that in astrophysical applications the shear (or differential rotation) can in general be a consequence of anisotropies in rotating systems. Our study can be also useful for understanding the origin of formation of the mesogranular structures in the solar convection (see Ref. 42).

[1] D. Etling and R. A. Brown, "Roll vortices in the planetary boundary layer: a review," Boundary-Layer Meteorol. **65**, 215 (1993).

[2] B. W. Atkinson and J. Wu Zhang, "Mesoscale shallow convection in the atmosphere," Rev. Geophys. **34**, 403 (1996).

[3] D. H. Lenschow and P. L. Stephens, "The role of thermals in the convective boundary layer," Boundary-Layer Meteorol. **19**, 509 (1980).

[4] J. C. R. Hunt, "Turbulence structure in thermal convection and shear-free boundary layers," J. Fluid Mech. **138**, 161 (1984).

[5] J. C. Wyngaard, "A physical mechanism for the asymmetry in top-down and bottom-up diffusion," J. Atmos. Sci. **44**, 1083 (1987).

[6] J. C. R. Hunt, J. C. Kaimal, and J. I. Gaynor, "Eddy structure in the convective boundary layer-new measurements and new concepts," Q. J. R. Meteorol. Soc. **114**, 837 (1988).

[7] H. Schmidt and U. Schumann, "Coherent structure in the convective boundary layer derived from large-eddy simulations," J. Fluid Mech. **200**, 511 (1989).

[8] S. S. Zilitinkevich, *Turbulent Penetrative Convection* (Avebury Technical, Aldershot, 1991), and references therein.

[9] A. G. Williams, H. Kraus, and J. M. Hacker, "Transport processes in the tropical warm pool boundary layer, Part I: Spectral composition of fluxes," J. Fluid Mech. **53**, 1187 (1996).

[10] S. S. Zilitinkevich, A. Grachev, and J. C. R. Hunt, "Surface frictional processes and non-local heat/mass transfer in the shear-free convective boundary layer," in *Buoyant Convection in Geophysical Flows*, edited by E. J. Plate, E. E. Fedorovich, and D. X. Viegas (Kluwer Academic, Dordrecht, 1998), pp. 83–113.

[11] B. Brümmer, "Roll and cell convection in winter-time arctic cold-air outbreaks," J. Atmos. Sci. **56**, 2613 (1999).

[12] G. S. Young, D. A. R. Kristovich, M. R. Hjelmfelt, and R. C. Foster, "Rolls, streets, waves and more," BAMS, July 2002, ES54.

[13] R. Krishnamurti and L. N. Howard, "Large-scale flow generation in turbulent convection," Proc. Natl. Acad. Sci. U.S.A. **78**, 1981 (1981).

[14] M. Sano, X. Z. Wu, and A. Libchaber, "Turbulence in helium-gas free convection," Phys. Rev. A **40**, 6421 (1989).

[15] S. Ciliberto, S. Cioni, and C. Laroche, "Large-scale flow properties of turbulent thermal convection," Phys. Rev. E **54**, R5901 (1996).

[16] L. P. Kadanoff, "Turbulent heat flow: structures and scaling," Phys. Today **54**, 34 (2001).

[17] J. J. Niemela, L. Skrbek, K. R. Sreenivasan, and R. J. Donnelly, "The wind in confined thermal convection," J. Fluid Mech. **449**, 169 (2001).

[18] J. J. Niemela and K. R. Sreenivasan, "Rayleigh-number evolution of large-scale coherent motion in turbulent convection," Europhys. Lett. **62**, 829 (2003).

[19] U. Burr, W. Kinzelbach, and A. Tsinober, "Is the turbulent wind in convective flows driven by fluctuations?," Phys. Fluids **15**, 2313 (2003).

[20] H. D. Xi, S. Lam, and X. Q. Xia, "From laminar plumes to organized flows: the onset of large-scale circulation in turbulent thermal convection," J. Fluid Mech. **503**, 47 (2004).

[21] X. D. Shang, X. L. Qiu, P. Tong, and X. Q. Xia, "Measurements of the local convective heat flux in turbulent Rayleigh-Benard convection," Phys. Rev. E **70**, 026308 (2004).

[22] E. Brown, A. Nikolaenko, and G. Ahlers, "Orientation changes of the large-scale circulation in turbulent Rayleigh-Bénard convection," Phys. Rev. Lett. **95**, 084503 (2005).

[23] A. Eidelman, T. Elperin, N. Kleeorin, A. Markovich, and I. Rogachevskii, "Hysteresis phenomenon in turbulent convection," Exp. Fluids **40**, 723 (2006).

[24] T. Hartlep, A. Tilgner, and F. H. Busse, "Large-scale structures in Rayleigh-Benard convection at high Rayleigh numbers," Phys. Rev. Lett. **91**, 064501 (2003).

[25] A. Parodi, J. von Hardenberg, G. Passoni, A. Provenzale, and E. A. Spiegel, "Clustering of plumes in turbulent convection," Phys. Rev. Lett. **92**, 194503 (2004).

[26] F. H. Busse and J. A. Whitehead, "Instabilities of convective rolls in a high Prandtl number fluid," J. Fluid Mech. **47**, 305 (1971).

[27] F. H. Busse and J. A. Whitehead, "Oscillatory and collective instabilities rolls in large Reynolds number convection," J. Fluid Mech. **66**, 67 (1974).

[28] F. H. Busse, "Generation of mean flows by thermal convection," Physica D **9**, 287 (1983).

[29] D. E. Fitzjarrald, "An experimental study of turbulent convection in air," J. Fluid Mech. **73**, 693 (1976).

[30] T. Elperin, N. Kleeorin, I. Rogachevskii, and S. S. Zilitinkevich, "Formation of large-scale semiorganized structures in turbulent convection," Phys. Rev. E **66**, 066305 (2002).

[31] T. Elperin, N. Kleeorin, I. Rogachevskii, and S. S. Zilitinkevich, "Tangling turbulence and semi-organized structures in convective boundary layers," Boundary-Layer Meteorol. **119**, 449 (2006).

[32] A. S. Monin and A. M. Yaglom, *Statistical Fluid Mechanics* (MIT Press, Cambridge, MA, 1975), and references therein.

[33] J. L. Lumley, "Rational approach to relations between motions of different scales in turbulent flows," Phys. Fluids **10**, 1405 (1967).

[34] J. C. Wyngaard and O. R. Cote, "Cospectral similarity in the atmospheric surface layer," Q. J. R. Meteorol. Soc. **98**, 590 (1972).

[35] S. G. Saddoughi and S. V. Veeravalli, "Local isotropy in turbulent boundary layers at high Reynolds number," J. Fluid Mech. **268**, 333 (1994).

[36] T. Ishihara, K. Yoshida, and Y. Kaneda, "Anisotropic velocity correlation spectrum at small scales in a homogeneous turbulent shear flow," Phys. Rev. Lett. **88**, 154501 (2002).

[37] W. H. Reid and D. L. Harris, "Some further results on the Bénard Problem," Phys. Fluids **1**, 102 (1958).

[38] S. Chandrasekhar, *Hydrodynamic and Hydromagnetic Stability* (Oxford Univ. Press, Oxford, 1961).

[39] P. G. Drazin, *Introduction to Hydrodynamic Stability* (Cambridge Univ. Press, Cambridge, 2002).

[40] D. Etling, "Some aspects on helicity in atmospheric flows," Contrib. Atmos. Phys. **58**, 88 (1985).

[41] I. Tuominen, A. Brandenburg, D. Moss, and M. Rieutord, "Does solar differential rotation arise from a large scale instability," Astron. Astrophys. **284**, 259 (1994).

[42] F. Cattaneo, D. Lenz, and N. Weiss, "On the origin of the solar mesogranulation," Astrophys. J. **563**, L91 (2001).